Early protoneutron star deleptonization - consistent modeling of weak processes and equation of state

2016 J. Phys.: Conf. Ser. 665 012069

(http://iopscience.iop.org/1742-6596/665/1/012069)

Early protoneutron star deleptonization - consistent modeling of weak processes and equation of state

T Fischer[1], L Huther[2], A Lohs[2] and G Martínez-Pinedo[2,3]

[1] Institute for Theoretical Physics, University of Wroclaw, pl. M. Borna 9, 50-204 Wroclaw, Poland
[2] Technische Universität Darmstadt, Schlossgartenstraße 2, 64289 Darmstadt, Germany
[3] GSI Helmholtzzentrum für Schwerionenforschung GmbH, Planckstraße 1, 64291 Darmstadt, Germany

E-mail: `fischer@ift.uni.wroc.pl`

Abstract. We discuss the impact of consistent modeling of weak processes and nuclear equation of state (EOS) during the deleptonization phase of protoneutron stars (PNS). They are born in the event of a core-collapse supernova. Being initially hot and lepton rich, PNSs deleptonize via the continuous emission of neutrinos of all flavors. Unlike during the mass accretion phase prior to the onset of the supernova explosion, when the neutrinospheres are located at low densities, they shift to significantly higher densities during the PNS deleptonization phase after the supernova explosion has been launched. Important during this phase is the inclusion of medium modifications to the weak processes, which depend on the nuclear EOS. In particular, these medium modifications depend on the nuclear symmetry energy and its density dependence. We discuss two selected nuclear models and illustrate the early PNS deleptonization phase for a particular EOS. As has been realized recently, including weak processes consistently with the EOS increases the spectral differences of ν_e and $\bar{\nu}_e$ in comparison to simulations that neglect the underlying medium modifications. This has important consequences for the nucleosynthesis relevant conditions of the ejecta as well as for potential neutrino flavor oscillations and hence detection on Earth.

1. Introduction

Stars more massive than about 8 $M_\odot$ end their life's as core-collapse supernovae [1, 2]. They are triggered from the collapse of the stellar core due to electron captures and the photodissociation of heavy nuclei. The collapse continues until normal nuclear matter density is reached. The nucleon pressure from the short-range repulsive nuclear interaction halts the collapse and the supersonically collapsing core bounces back. A sound wave turns into a shock wave which then propagates out of the core. The object which forms at core bounce is the protoneutron star (PNS), being hot and lepton rich in which senses it differs form the final supernova remnant, the neutron star. The moment of core bounce is determined when the maximum central density is reached just before shock break out. The initially outwards propagating bounce shock finally halts due to energy losses from the dissociation of heavy nuclei, which fall onto the shock from the still gravitationally collapsing region above the core, and electron neutrino escapes. The latter are released in the deleptonization burst which is launched from a large number of electron captures on free protons when the bounce shock propagates across the neutrinospheres. The ν_e-luminosity reaches several times 10^{53} erg s^{-1} and lasts only about 10–20 ms after core

bounce. These sources of energy loss turn the bounce shock into an accretion front which stalls at about 100–200 km. The revival of this shock wave, the so called supernova problem, is related to the liberation of energy from the central PNS into the layer above the PNS surface behind the standing shock. Several scenarios have been explored in the literature, the magneto-rotational [3], the acoustic [4], the high-density quark-hadron phase transition [5], and the neutrino heating [6]. The moment of explosion onset can be defined when the standing accretion shock starts to propagate continuously to increasingly larger radii and does not retreat back at any later times. It will expel the stellar mantel, ejecting manly α-nuclei up to the iron group.

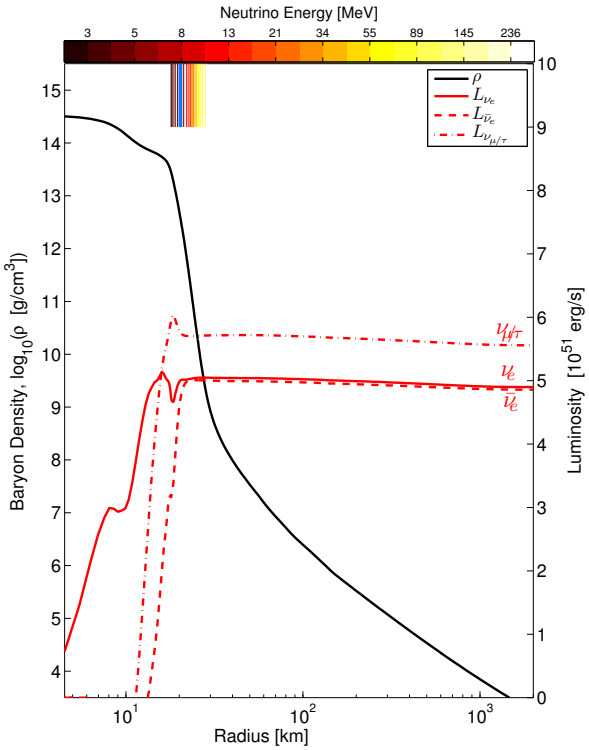

$$\nu_e + n \longrightarrow e^- + p \quad \text{(1a)}$$

$$\bar{\nu}_e + p \longrightarrow e^+ + n \quad \text{(1b)}$$

$$\nu + N \longrightarrow \nu' + N \quad \text{(1c)}$$

$$\nu + e^{\pm} \longrightarrow \nu' + e^{\pm} \quad \text{(1d)}$$

$$N + N \longrightarrow \nu + \bar{\nu} + N + N \quad \text{(1e)}$$

$$e^- + e^+ \longrightarrow \nu + \bar{\nu} \quad \text{(1f)}$$

$$\nu_e + \bar{\nu}_e \longrightarrow \nu_{\mu/\tau} + \bar{\nu}_{\mu/\tau} \quad \text{(1g)}$$

$$(N = \{n, p\})$$

$$(\nu = \{\nu_e, \nu_{\mu/\tau}\} \quad \text{unless stated otherwise})$$

Figure 1. Left column: Radial profiles of density (solid black line) and luminosities (ν_e: solid red line, $\bar{\nu}_e$: dashed red line, $\nu_{\mu/\tau}$: dash-dotted line) at about 2 s after explosion onset. The region of neutrino decoupling is shown via the energy-dependent transport spheres (for ν_e), where the color-coding is according to the neutrino energies from $E_{min} = 3$ MeV (black) at about 16.17 km up to $E_{max} = 300$ MeV (white) at 49.11 km. The energy-averaged ν_e-sphere is shown in the vertical blue solid line. (color online) Right column: List of weak processes.

Independent from the shock-revival mechanism, a layer of net neutrino heating establishes above the PNS surface after the explosion has been launched. It drives a low-mass ($\sim 10^{-4}$ M$_\odot$) outflow, known as neutrino-driven wind. It has been explored in parametric [7, 8, 9, 10] as well as in dynamic studies [11, 12, 13, 14]. It has also long been investigated as nucleosynthesis site for the production of both, light p-nuclei and r-process nuclei [15, 16, 17]. One of the largest uncertainties of neutrino-driven winds is the proton-to-baryon ratio Y_e, which is determined by the weak processes (1a) and (1b) at the neutrinospheres. Addressing this question requires neutrino transport to accurately describe neutrino decoupling from matter at the PNS surface. It determines the neutrino spectra and luminosities and hence the nucleosynthesis relevant

conditions in the wind at larger radii [18]. Note that process (1a) will turn matter to the proton-rich side, while process (1b) will turn matter to the neutron-rich side. Moreover, material at neutrino decoupling is extremely neutron rich yielding $Y_e \simeq 0.05 - 0.1$, as a consequence of the deleptonization burst form core bounce. In order to achieve neutron-rich conditions for the material being ejected from the PNS surface in the neutrino-driven wind, it has been demonstrated analytically that for similar ν_e and $\bar{\nu}_e$ luminosities, $\langle E_{\bar{\nu}_e}\rangle - \langle E_{\nu_e}\rangle \sim 5$ MeV [18]. In recent spherically symmetric simulations that are based on general relativistic radiation hydrodynamics and accurate three-flavor Boltztmann neutrino transport [19, 20], it has been found that $\langle E_{\bar{\nu}_e}\rangle - \langle E_{\nu_e}\rangle \sim 2 - 3$ MeV, decreasing towards later times during the ongoing PNS deleptonization. The simulations were carried out for more than 10 s after explosion onset during which generally $Y_e > 0.5$ was found.

In the following section, we will discuss this aspect and demonstrate the complexity of the situation. In particular, we will point to the importance of the consistent implementation of rates for weak processes and nuclear equation of state (EOS). This was not the case in the studies of refs. [19, 20], as has been pointed out very recently in refs. [21, 22].

2. Protoneutron star deleptonization and role of charged-current weak processes

A typical situation during the early PNS deleptonization phase is illustrated in the left panel of Fig. 1 at about 2 s after the explosion has been launched. Note the very steep density profile at the PNS surface, where neutrino decoupling takes place over 5 orders of magnitude in density, which even steepens during the continuous deleptonization. In this region (see the neutrino decoupling in the left panel of Fig. 1) neutrino transport is important to determine the neutrino spectra and luminosities. The magnitude of the luminosity and average energy differences depends on details of the neutrino transport and in particular on the weak processes and their implementation. In addition to the charged-current weak processes, other weak processes are important which are listed in the right panel of Fig. 1. These are neutral current elastic (exchange of momentum) scattering on nucleons (1c), inelastic (exchange of energy and momentum) scattering on electrons/positrons (1d), and pair processes (1e-1g).

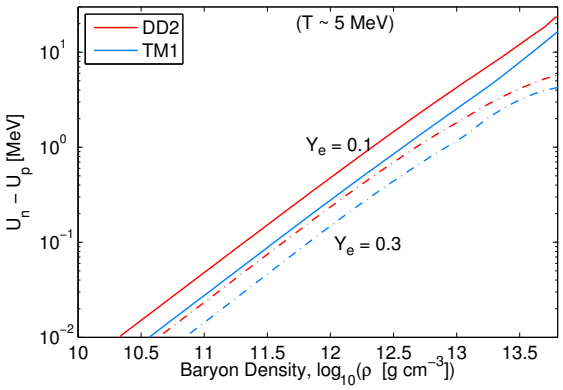

Figure 2. Density dependence of the mean-field potential difference for two selected nuclear interactions DD2 (red lines) and TM1 (blue lines), comparing different proton-to-baryon ratios $Y_e = 0.1$ (solid lines) and $Y_e = 0.3$ (dash-dotted lines) at fixed temperature of about 5 MeV. With increasing isospin asymmetry, i.e. lower Y_e, the differences between U_n and U_p become larger. (color online)

The rate for the charged current process (1a) can be expressed via momentum integrals of the particle occupation numbers, F_i, and the spin-averaged squared matrix element, M, in the zero-momentum transfer approximation ($\mathbf{p}_n \simeq \mathbf{p}_p$) [24, 25]:

$$1/\lambda(E_{\nu_e}) \simeq \frac{G_F^2}{\pi} V_{ud}^2 (g_V^2 + 3g_A^2) \cdot E_e^2 [1 - f_e(E_e)] \frac{n_n - n_p}{1 - e^{\beta(\mu_p^0 - \mu_n^0)}}, \qquad (2)$$

with Fermi constant, G_F, vector and axial-vector coupling constants, g_V and g_A, and up-down entry of the Cabibbo-Kobayashi-Maskawa matrix V_{ud}. A similar expression is obtained

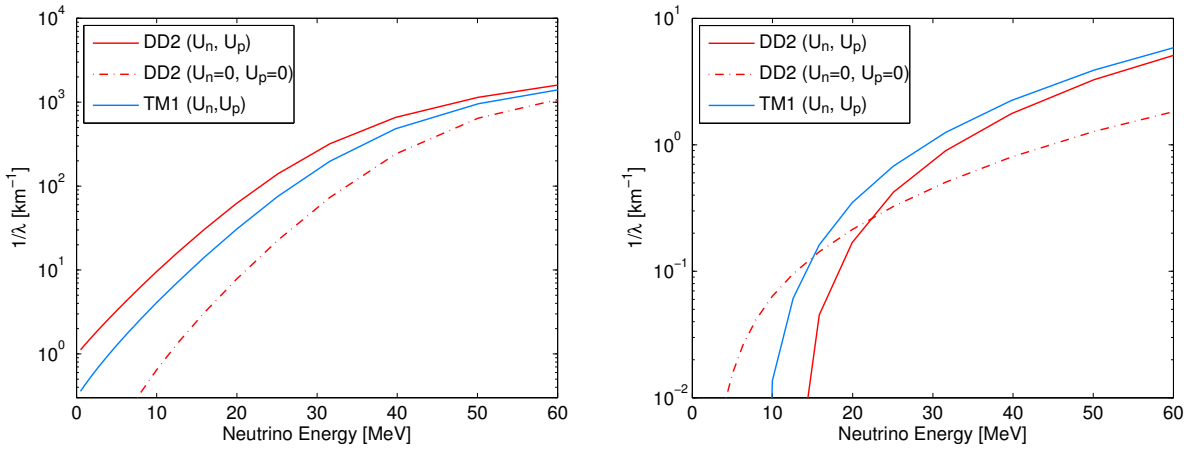

(a) ν_e (b) $\bar{\nu}_e$

Figure 3. Neutrino opacity (Eq. 2) for the two interactions DD2 (solid red lines) and TM1 (solid blue lines) at selected conditions [23], $T = 7.4$ MeV, $\rho = 2.1 \times 10^{13}$ g cm^{-3}, and $Y_e = 0.035$. It corresponds to $U_n - U_p = 10.5(6.5)$ MeV for DD2(TM1). In addition, the red dashed line shows the opacity for DD2 for which we assume zero potentials. (color online)

for reaction (1b). For the reverse process, i.e. the neutrino emissivity, detailed balance is applied, $j_{\nu_e}(E_{\nu_e}) = \exp\{-\beta(E_{\nu_e} - \mu^{\rm eq.}_{\nu_e})\}\, 1/\lambda(E_{\nu_e})$ with equilibrium chemical potential $\mu^{\rm eq.}_{\nu_e} = \mu_e - (\mu_n - \mu_p)$ and inverse temperature $\beta = 1/T$. Expression (2) assumes the free Fermi gas of nucleons, i.e. in the limit of low degeneracy the nucleon density of targets, n_N, must be recovered. Hence, the nucleon chemical potentials, μ^0_N, that enter in (2) must be those of the free Fermi gas. In supernova codes, these quantities are typically provided by an EOS based on some nuclear interaction model. Nucleons are treated as quasi-particles that move in a potential, U_N, and obey the following dispersion relation,

$$E_N(\mathbf{p}_N) = \sqrt{\mathbf{p}_N^2 + {m^*_N}^2} + U_N, \qquad (N = \{n, p\}). \tag{3}$$

In the case of uniform matter the single-particle potentials are given by the vector self energy. They and the effective masses, m^*_N, depend on the independent variables density, temperature, and Y_e, such as the entire EOS. Consequently, the nuclear chemical potentials which enter Eq. (2) must be corrected accordingly in order to reproduce the non-interacting case, i.e. $\mu^0_N = \mu_N - U_N - m^*_N$ where μ_N are the full potentials that contain contributions from interactions. Moreover, since neutrino transport uses charged-current reaction rates with respect to the incoming neutrino energy, E_{ν_e} (see Eq. 2), Eq. (3) can be used to relate electron(positron) energy, $E_{e^-}(E_{e^+})$, and electron (anti)neutrino energy for processes (1a) and (1b) as follows,

$$E_{\nu_e} = E_{e^-} - (m_n - m_p) - (U_n - U_p), \qquad E_{\bar{\nu}_e} = E_{e^+} + (m_n - m_p) + (U_n - U_p). \tag{4, 5}$$

From the expressions (4) and (5) it becomes clear that at low densities, where $U_n - U_p \simeq 100$ keV (see Fig. 2), the energetics is determined by the vacuum Q-value, $Q_0 = m_n - m_p = 1.2935$ MeV. The density dependence of the quantity $U_n - U_p$ is shown in Fig. 2 for selected Y_e and at fixed temperature of about 5 MeV. The figure also compares two nuclear interaction models, DD2 [26] and TM1 from the comprehensive supernova catalog of ref. [27] which is based on the statistical model including detailed nuclear composition consistently and have been approved in supernova simulations [28, 29].

The ν_e and $\bar{\nu}_e$-opacity are shown in Figs. 3(a) and 3(b), at selected conditions. From the figures one immediately realizes that neglecting (U_n, U_p) leads to a suppression of low-energy neutrino absorptions (compare the red solid and dash-dotted lines) for ν_e. The magnitude scales almost with $U_n - U_p$. This is attributed mainly to the modified vacuum Q-value and also partly to the chemical potential modifications. For $\bar{\nu}_e$ the opposite holds due to the different sign of the modified vacuum Q-value, including the mean-field potentials leads to a suppression of low $\bar{\nu}_e$ energies. In addition to DD2, Fig. 3 also shows the opacity for TM1 (blue lines), with lower mean-field potentials of about 4 MeV at the same conditions. Hence, also the opacity for ν_e is reduced accordingly, and increased for $\bar{\nu}_e$. Note that the opacity differences between DD2 and TM1 are not entirely due to the different (U_n, U_p) but also related in part to their different neutron and proton abundances.

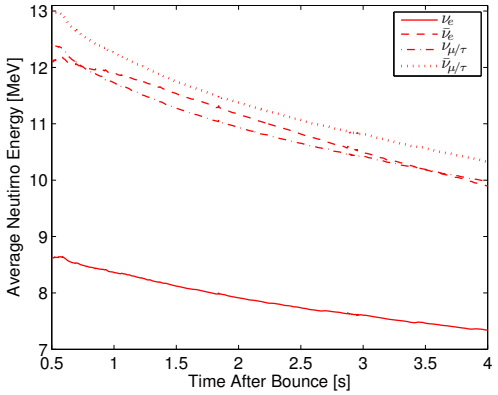

(a) Average neutrino energies.

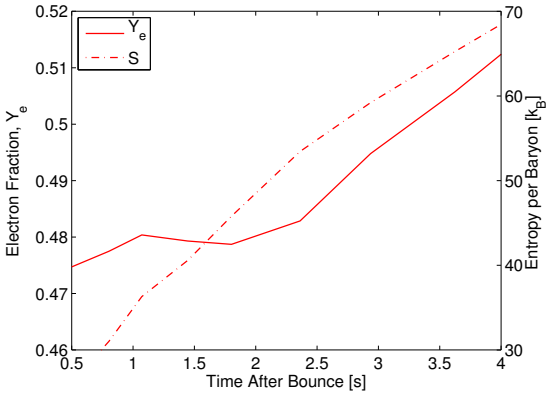

(b) Electron fraction and entropy per baryon.

Figure 4. Evolution of neutrino energies, Y_e, and entropy per baryon (both obtained in large nucleosynthesis calculations) sampled at a distance of 1000 km. Neutron-rich conditions are obtained between 1.5–2.5 s when the differences between $\langle E_{\bar{\nu}_e} \rangle$ and $\langle E_{\nu_e} \rangle$ are largest.

The impact of the consistent implementation of charged-current weak rates and EOS in simulations of the PNS deleptonization has been shown in refs. [21, 22] for the neutrino spectra and luminosities, as well as the resulting nucleosynthesis relevant conditions. It was found that it leads to generally larger differences of the average energies and luminosities for ν_e and $\bar{\nu}_e$. Here we extend the analysis of ref. [21] and simulate a 11.2 $M_\odot$ progenitor applying our general relativistic radiation hydrodynamics code AGILE-*Boltztran*, which is based on three-flavor Boltzmann neutrino transport [30]. We model a neutrino-driven explosion in our spherically symmetric setup by enhancing the neutrino heating/cooling rates (for details, see ref. [19]). Fig. 4 shows the results obtained for the early PNS deleptonization phase where the charged-current weak rates are implemented consistently with the nuclear EOS DD2. During this early epoch, slightly neutron-rich conditions are found up to about 3 s after bounce. It allows for the production of light neutron-capture elements up to $Z \simeq 45$ but no strong r process. The rising Y_e at later times is related to the reducing opacity of the charged-current reactions, due to the increasing importance of final-state Pauli blocking and the increasing nucleon degeneracy [23]. Instead, elastic scattering on neutrons starts to dominates the opacity, which does not distinguish between different neutrino flavors and hence the spectral differences reduce.

3. Conclusions

We have discussed the consistent implementation of charged-current weak rates and nuclear EOS in radiation hydrodynamics codes and its relevance during the early PNS cooling phase.

The weak rates have now a direct dependence on the nuclear EOS. We have employed rates based on the zero-momentum transfer approximation. It is a valid simplification since inelastic contributions are small for the early deleptonization phase, during which the neutrinospheres are located at intermediate densities $\sim 10^{13}$ g cm^{-3}. Inelastic contributions, as well as nuclear correlations [31], may become of some relevance during the later evolution when the neutrino decoupling region moves to even higher densities ($\sim 10^{14}$ g cm^{-3}). Moreover, corrections due to weak magnetism, which also have to be consistent with the EOS, are not included. Long-term simulations up to 10 s are required to cover the entire PNS deleptonization phase and to study the late neutrino-driven wind, also with particular focus on the nucleosynthesis.

One of the currently largest uncertainties in such studies is the nuclear EOS, in particular at high densities, finite temperatures and low Y_e. Future explorations will also study the impact of different EOS on the PNS deleptonization. E.g., soft EOS that lead typically to a more compact PNS have also a lower symmetry energy. Since the medium modifications to the charged-current rates, $U_n - U_p$, depend sensitively on the symmetry energy also at intermediate densities, a direct impact on the PNS deleptonization can be expected.

TF is supported by the Narodowe Centrum Nauki (NCN) within the "Maestro" program under contract No. DEC-2011/02/A/ST2/00306. GMP, LH, and AL are partly supported by the Deutsche Forschungsgemeinschaft through contract SFB 634, the Helmholtz International Center for FAIR within the framework of the LOEWE program launched by the state of Hesse, the Helmholtz Association through the Nuclear Astrophysics Virtual Institute (VH-VI-417)

References

[1] Janka H T, Langanke K, Marek A, Martínez-Pinedo G and Müller B 2007 *Phys. Rep.* **442** 38–74
[2] Janka H T 2012 *Annual Review of Nuclear and Particle Science* **62** 407–451
[3] LeBlanc J M and Wilson J R 1970 *Astrophys.J.* **161** 541
[4] Burrows A, Livne E, Dessart L, Ott C and Murphy J 2006 *Astrophys.J.* **640** 878–890
[5] Sagert I, Fischer T, Hempel M, Pagliara G, Schaffner-Bielich J *et al.* 2009 *Phys.Rev.Lett.* **102** 081101
[6] Bethe H A and Wilson James R 1985 *Astrophys.J.* **295** 14–23
[7] Duncan R C, Shapiro S L and Wasserman I 1986 *Astrophys. J.* **309** 141–160
[8] Hoffman R, Woosley S and Qian Y 1997 *Astrophys.J.* **482** 951
[9] Thompson T A, Burrows A and Meyer B S 2001 *Astrophys.J.* **562** 887
[10] Thompson T A and Burrows A 2001 *Nucl.Phys.* **A688** 377–381
[11] Woosley S E and Baron E 1992 *Astrophys. J.* **391** 228–235
[12] Woosley S, Wilson J, Mathews G, Hoffman R and Meyer B 1994 *Astrophys.J.* **433** 229–246
[13] Takahashi K, Witti J and Janka H T 1994 *Astron.Astrophys.* **286** 857
[14] Witti J, Janka H T and Takahashi K 1994 *Astronom. Astrophys.* **286** 841–856
[15] Otsuki K, Tagoshi H, Kajino T and Wanajo S 1999 *Astrophys.J.* **533** 424
[16] Wanajo S 2006 *Astrophys.J.* **650** L79–L82
[17] Wanajo S 2006 *Astrophys.J.* **647** 1323–1340
[18] Qian Y and Woosley S 1996 *Astrophys.J.* **471** 331–351
[19] Fischer T, Whitehouse S, Mezzacappa A, Thielemann F K and Liebendörfer M 2010 *Astron.Astrophys.* **517** A80
[20] Hüdepohl L, Müller B, Janka H T, Marek A and Raffelt G G 2010 *Physical Review Letters* **104** 251101
[21] Martínez-Pinedo G, Fischer T, Lohs A and Huther L 2012 *Physical Review Letters* **109** 251104
[22] Roberts L F, Reddy S and Shen G 2012 *Phys. Rev. C* **86** 065803
[23] Fischer T, Martínez-Pinedo G, Hempel M and Liebendörfer M 2012 *Phys. Rev. D* **85** 083003
[24] Bruenn S W 1985 *Astrophys.J.Suppl.* **58** 771–841
[25] Reddy S, Prakash M and Lattimer J M 1998 *Phys. Rev. D* **58** 013009
[26] Typel S 2005 *Phys. Rev. C* **71** 064301
[27] Hempel M and Schaffner-Bielich J 2010 *Nucl.Phys.* **A837** 210–254
[28] Hempel M, Fischer T, Schaffner-Bielich J and Liebendörfer M 2012 *Astrophys. J.* **748** 70
[29] Steiner A W, Hempel M and Fischer T 2013 *Astrophys. J.* **774** 17
[30] Liebendörfer M, Messer O, Mezzacappa A, Bruenn S, Cardall C *et al.* 2004 *Astrophys.J.Suppl.* **150** 263–316
[31] Reddy S, Prakash M, Lattimer J M and Pons J A 1999 *Phys. Rev. C* **59** 2888–2918